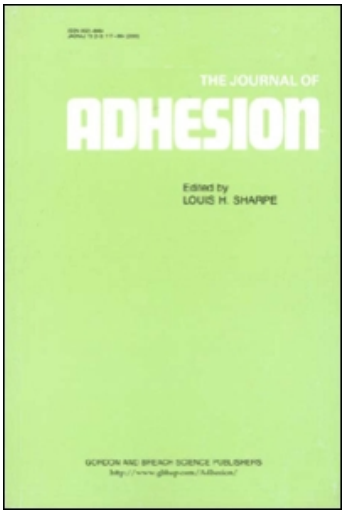

The Journal of Adhesion
Publication details, including instructions for authors and subscription information:
http://www.informaworld.com/smpp/title~content=t713453635

Repair of Wood Trusses Loaded in Tension with Adhesively Bonded Carbon-Epoxy Patches

A. M. J. P. Barreto[a]; R. D. S. G. Campilho[b]; M. F. S. F. de Moura[b]; J. J. L. Morais[c]; C. L. Santos[c]
[a] Instituto de Engenharia Mecânica e Gestão Industrial, Universidade do Porto, Porto, Portugal [b] Faculdade de Engenharia da Universidade do Porto, Departamento de Engenharia Mecânica, Universidade do Porto, Porto, Portugal [c] CITAB/UTAD, Departamento de Engenharias, Vila Real, Portugal

Online publication date: 10 June 2010

To cite this Article Barreto, A. M. J. P. , Campilho, R. D. S. G. , Moura, M. F. S. F. de , Morais, J. J. L. and Santos, C. L.(2010) 'Repair of Wood Trusses Loaded in Tension with Adhesively Bonded Carbon-Epoxy Patches', The Journal of Adhesion, 86: 5, 630 — 648
To link to this Article: DOI: 10.1080/00218464.2010.484316
URL: http://dx.doi.org/10.1080/00218464.2010.484316

The Journal of Adhesion, 86:630–648, 2010

ISSN: 0021-8464 print/1545-5823 online
DOI: 10.1080/00218464.2010.484316

Taylor & Francis
Taylor & Francis Group

Repair of Wood Trusses Loaded in Tension with Adhesively Bonded Carbon-Epoxy Patches

A. M. J. P. Barreto[1], R. D. S. G. Campilho[2], M. F. S. F. de Moura[2], J. J. L. Morais[3], and C. L. Santos[3]
[1]Instituto de Engenharia Mecânica e Gestão Industrial, Universidade do Porto, Porto, Portugal
[2]Faculdade de Engenharia da Universidade do Porto, Departamento de Engenharia Mecânica, Universidade do Porto, Porto, Portugal
[3]CITAB/UTAD, Departamento de Engenharias, Vila Real, Portugal

Wood and wood products are amongst the most important construction materials. Wood is generally used in frames, buildings, truss roof structures in buildings, bridges, towers, railroad infrastructures, and many more applications. Damage and failure behaviour of wood members in tensile, compressive, or shear loading are extremely important to account for in wooden structures subjected to high working stresses. Wood exhibits its greatest strength in tension in the grain direction. A few applications load a wood member in pure tension, such as trusses in the most varied applications. For a safe design, predictive methods and models for the simulation of the structural behaviour of these elements are required. One of the possible approaches is the finite element method. In this work, the tensile strength of adhesively bonded repairs with carbon-fibre reinforced plastic patches on wood members in pure tension is addressed experimentally and numerically. A parametric analysis was carried out on the overlap length (L_O) between the composite reinforcement and the undamaged region of the beam. The numerical analysis used the finite element method and cohesive zone models to simulate damage initiation and propagation in different materials such as the adhesive or wood in different propagation planes. The comparative analysis of the test results and the simulations showed a good correlation between both and provided design principles for these structures. An optimization technique to reduce stress concentrations and eventually increase the repair's strength was also tested numerically,

Received 22 June 2009; in final form 30 January 2010.
Presented in part at the 3rd International Conference on Advanced Computational Engineering and Experimenting (ACE-X 2009), Rome, Italy, 22–23 June 2009.
Address correspondence to M. F. S. F. de Moura, Faculdade de Engenharia da Universidade do Porto, Departamento de Engenharia Mecânica, Rua Dr. Roberto Frias s/n, 4200-465 Porto, Portugal. E-mail: mfcoura@fe.up.pt

consisting of adhesive filleting at the patch edges. Results showed that this technique can be used to increase the strength of the repairs.

Keywords: Cohesive Zone Models; Composite; Finite Element Analysis; Repair; Wood

1. INTRODUCTION

Wood trusses are engineered components widely used in residential, institutional, agricultural, and commercial construction. Although trusses are slender elements, they are very strong when placed in the vertical position because they make use of the most efficient geometric shape we know of—the triangle. But if racked or bent in the lateral direction, they can be easily damaged or broken. This damage or failure in tensile, compressive, or shear loading can occur at the joints (connector plates) or within the lumber members and is extremely important to account for in wooden structures subjected to high working stresses. In order to spread loads, wood or metal members are placed between trusses and joints in an angled position. Wood exhibits its greatest strength in tension parallel to the grain, but in reality there are only a few applications where pure tension loading conditions prevail. But this material is generally weak in tension perpendicular to the grain. So, it is imperative to study the behaviour of wood to give structural designers some insurance in the various applications in which this material can be applied.

Wood has been recognised as an orthotropic material [1]. It is one of the oldest materials used in construction and presents many advantages, such as that it is a natural and renewable resource and relatively inexpensive. However, its biological origin gives wood a variable and heterogeneous behaviour and its mechanical properties are affected by the presence of knots, checks, shakes, splits, slope of grain, reaction wood and decay, etc. [2]. Reinforcement is one of the ways of improving mechanical behaviour of wood. There is a considerable number of studies using metallic reinforcement [3–11]. The first time carbon fiber-reinforced plastic (CFRP) was used as tension reinforcement of wood was in 1992 [12]. The cost of CFRP is relatively high, so prestressing the FRP sheets before applying them through external bonding on the tension zones of wood surface was considered a justified measure [13]. Repairing techniques are also used for large-scale wood structures, but only a few studies have been published using the adhesive-bonding technique [14–20]. This technique is identified as the most efficient method of stress transfer between FRP and wood, as it avoids the stress concentrations due to mechanical fasteners [21].

Moreover, assembly costs are lower and involve just a few finishing operations. Fiorelli and Dias [22] studied the application of glass and carbon fibers in the reinforcement and recovery of timber beams. The authors came to the conclusion that it is a viable option not only because it is easy to do but also that it confers the greater strength and stiffness of reinforced structural elements and reduces the possibility of tensile failure caused by defects. Humphreys and Francey [15] studied the use of carbon fibre composite materials to rehabilitate timber structures and reported that the failure of the test specimens occurred due to delamination of the carbon fibre laminates. The authors also concluded that further investigation into the ability of the carbon fibre strips to bond to the timber is required. Campilho *et al.* [23] presented an experimental and numerical study concerning the fracture of scaled specimens of wood beams repaired with a carbon-epoxy patch under four-point bending. The technique consisted of removing a semi-circular shape of the damaged wood material that existed at the compression region of an intermediate section and placing an a adhesively-bonded carbon-epoxy patch.

In this work, the tensile strength of adhesively-bonded repairs with CFRP patches on wood members of the *Pinus Pinaster* species was addressed experimentally and numerically. A wood beam such as a truss element under tension is supposed to have suffered any kind of damage, such as tensile failure induced by overloads, natural decay, or human intervention. The repair consists of the replacement of the damaged wood undamaged portion with an insert of the same material, adhesively-bonded between the undamaged wood portions, and reinforcement with CFRP patches bonded at two opposite faces. A parametric analysis was carried out on the value of L_O (the length between the composite reinforcement and the undamaged part of the beam). The numerical analysis used the finite element method (FEM) and cohesive zone models (CZMs) to simulate damage initiation and propagation in different materials. An epoxy adhesive particularly suited to bond CFRP and wood was selected for the repairs (Araldite® 2015 from Huntsman, Basel, Switzerland). This adhesive, as most structural adhesives used nowadays, is characterized by extensive plasticization in tension and shear following its elastic region. Thus, trapezoidal cohesive laws [24] in each pure mode were used for a faithful simulation of its ductility. To account for the experimental failures, damage propagation in the wood beam was also simulated along two different planes. Following the parametric study on L_O, an optimization technique to reduce stress concentrations was tested numerically in an attempt to increase the strength of the repairs. This method consisted of adhesive filleting at the patch edges.

2. COHESIVE ZONE MODEL (CZM)

2.1. Model Description

A mixed-mode (I + II) CZM implemented within cohesive elements was used to simulate an adhesive layer of Araldite 2015 with thickness (t_A) of 0.2 mm. A trapezoidal law between stresses ($\boldsymbol{\sigma}$) and relative displacements ($\boldsymbol{\delta}_r$) between homologous points of the cohesive elements with zero thickness was considered (Fig. 1) to account for the adhesive ductility [24–26]. This law was also used with some modifications to simulate the wood fractures. The formulation allows a mixed-mode behaviour, in which damage onset is predicted using the quadratic stress criterion

$$\begin{aligned} &\left(\frac{\sigma_{\mathrm{I}}}{\sigma_{\mathrm{u,I}}}\right)^2+\left(\frac{\sigma_{\mathrm{II}}}{\sigma_{\mathrm{u,II}}}\right)^2=1 \quad \text{if } \sigma_{\mathrm{I}}>0 \\ &\sigma_{\mathrm{II}}=\sigma_{\mathrm{u,II}} \qquad\qquad\qquad\quad \text{if } \sigma_{\mathrm{I}}\le 0 \end{aligned}, \tag{1}$$

where σ_i (i = I, II) represent the stresses in each mode and $\sigma_{u,i}$ (i = I, II) the corresponding local strength. Taking into account that stresses, σ_i, and relative displacements, δ_i, are related by means of the interface stiffness, d_i, *i.e.*, $\sigma_i = d_i\delta_i$, Eq. (1) can be rewritten as a function of the relative displacements considering that

$$\left(\frac{\delta_{1\mathrm{m,I}}}{\delta_{1,\mathrm{I}}}\right)^2+\left(\frac{\delta_{1\mathrm{m,II}}}{\delta_{1,\mathrm{II}}}\right)^2=1. \tag{2}$$

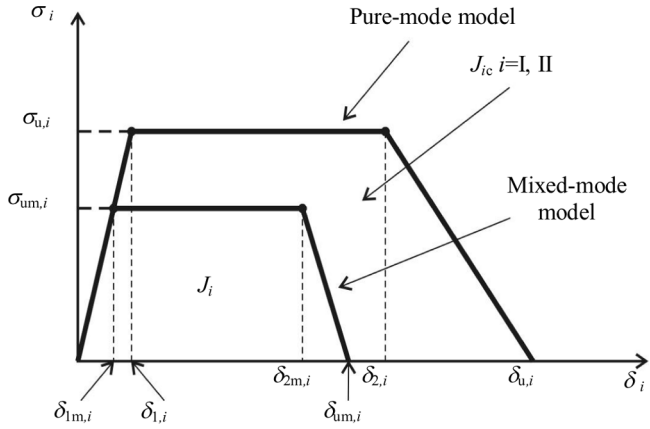

FIGURE 1 The trapezoidal softening law for pure-mode and mixed-mode.

$\delta_{1,i}$ ($i = \mathrm{I}$, II) are the pure-mode relative displacements at damage initiation and $\delta_{1\mathrm{m},i}$ ($i = \mathrm{I}$, II) the corresponding mixed-mode ones (Fig. 1). Stress softening onset was predicted using a criterion similar to Eq. (2):

$$\left(\frac{\delta_{2\mathrm{m,I}}}{\delta_{2,\mathrm{I}}}\right)^2 + \left(\frac{\delta_{2\mathrm{m,II}}}{\delta_{2,\mathrm{II}}}\right)^2 = 1. \tag{3}$$

$\delta_{2,i}$ ($i = \mathrm{I}$, II) are the relative displacements in pure-mode at stress softening onset and $\delta_{2\mathrm{m},i}$ ($i = \mathrm{I}$, II) the corresponding mixed-mode ones (Fig. 1). Crack growth was simulated by the linear energetic criterion [24]:

$$\frac{J_{\mathrm{I}}}{J_{\mathrm{Ic}}} + \frac{J_{\mathrm{II}}}{J_{\mathrm{IIc}}} = 1. \tag{4}$$

J_{ic} ($i = \mathrm{I}$, II) is the fracture energy in the respective pure mode and corresponds to the area of the bigger trapezoid in Fig. 1. J_i ($i = \mathrm{I}$, II) represents the energy dissipated in each mode and is given by the area of the small trapezoid in Fig. 1. When Eq. (4) is satisfied at a given integration point damage grows and stresses are released, with the exception of normal compressive ones. A detailed description of this model can be found in the work of Campilho *et al.* [27].

2.2. Fracture Simulation

To model a cohesive crack propagation in a $t_{\mathrm{A}} = 0.2\,\mathrm{mm}$ layer of the ductile adhesive Araldite 2015, a trapezoidal relationship was established (Fig. 1). In these cohesive laws, the quantities $\sigma_{\mathrm{u},i}$ and J_{ic} ($i = \mathrm{I}$, II) are the most important parameters for the accuracy of the results from the simulations [28]. The mechanical properties of adhesive layers vary markedly with the value of t_{A}, being also different from the adhesive bulk properties [29,30]. This variation can be ascribed to the influence of the surrounding adherends on the height and extension of the fracture process zone (FPZ) [29,31,32]. In this work, for a faithful characterization of the adhesive layer, its cohesive laws in pure-Modes I and II were estimated by double cantilever beam (Mode I) and end-notched flexure (Mode II) tests with the same value of t_{A} used in the repairs. An inverse modelling technique was employed for the extraction of the values of $\sigma_{\mathrm{u},i}$ and $\delta_{2,i}$, after J_{ic} was estimated by appropriate data reduction schemes [33,34]. The adhesive layer elastic stiffness in tension and shear (up to $\delta_{1,i}$, Fig. 1) was specified from the experimentally measured values of Young's modulus ($E = 1850\,\mathrm{MPa}$) and shear modulus ($G = 650\,\mathrm{MPa}$) [35]. A

TABLE 1 Cohesive Parameters in Pure Modes I and II Used to Simulate Different Failures

Cohesive laws	i	J_{ic} [N/mm]	$\sigma_{u,i}$ [MPa]	$\delta_{2,i}$ [mm]	$\delta_{u,i}$ [mm]
Adhesive layer [33,34]	I	0.43	23.0	0.0187	0.021
	II	4.70	22.8	0.1710	0.248
Wood in the *RL* plane [36]	I	0.2	16	1.6×10^{-5}	0.025
	II	1.2	16	1.6×10^{-5}	0.150
Wood in the *LR* plane	I	25	65	6.5×10^{-5}	0.77
	II	1.2	16	1.6×10^{-5}	0.15

detailed description of this procedure is given in the work of Campilho *et al.* [27]. Apart from the adhesive layer, damage growth within the wood beam was also considered, horizontally as an *RL* propagation (in the horizontal longitudinal plane of the beam) and transversely as an *LR* propagation (cross-sectional fracture of the beam). It should be noted that crack propagation systems in wood are identified by a pair of letters: the first one gives the direction of the normal to the crack plane and the second indicates the direction of crack propagation. For the crack growth modelling of these propagations using cohesive elements, some adjustments to the trapezoidal laws were made to simulate the brittle fracture of wood. These included the conversion to a triangular shape (making $\delta_{2,i} = \delta_{1,i}$ in Fig. 1) and using a penalty function method up to $\sigma_{u,i}$ (Fig. 1). The cohesive parameters for this species of wood were obtained from a previous work of the authors [36]. A summary of all cohesive parameters is presented in Table 1.

3. EXPERIMENTAL WORK

Figure 2 shows the repair geometry and characteristic dimensions. A wood beam under tension (*e.g.*, a truss element) is supposed to have suffered any kind of damage, such as tensile failure induced by overloads, natural decay, or human intervention. The repair initially consists of the removal of the damaged wood portion by cutting of a small portion of the member transversely to its length. An insert of the same wood species is then adhesively-bonded between the two broken segments of the truss, in order to preserve the length of the beam before repair. To achieve the restitution of the initial strength, this solution is clearly ineffective since the properties of epoxy adhesives in tension are much lower than the strength of wood in the fibres' length direction (*L*-direction). Thus, reinforcement of the beam is accomplished by adhesively bonding thin CFRP patches at opposite faces of the wood

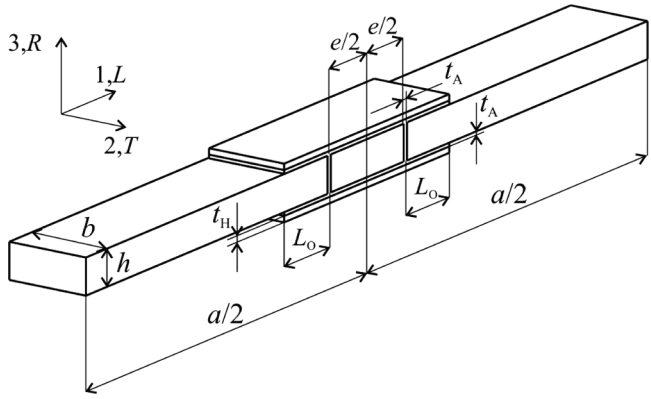

FIGURE 2 Schematic representation of the repair with the characteristic dimensions.

member. In the experiments, the undamaged beam strength was also evaluated to allow the definition of the value of L_O that fully restores the beam's strength. The axes 1,2,3 of Fig. 2 correspond to the fibre, transverse, and thickness directions of the CFRP patch, respectively. The *R,L,T* coordinate system pertains to the wood orientations [fibres longitudinal direction (*L*), rings radial direction (*R*), and rings tangential direction (*T*)]. The repair dimensions were chosen in order to represent typical specimens used for wood characterization. They are (in mm): the beam's width ($b = 20$), thickness ($h = 10$), and length ($a = 200$), the removed portion length ($e = 20$), the patch thickness ($t_H = 0.6$), the adhesive thickness ($t_A = 0.2$), and L_O (5, 10, and 15). The value of a relates to the spacing between the testing machine grips. To avoid crushing and slipping of the specimens, tabs of a harder wood species were bonded at the edges of the specimens, comprising an attachment length of 50 mm. Under the proposed testing conditions, the patch will be mainly under uniaxial tension. For an optimization of the repair and minimization of costs, the patch consisted of a unidirectional lay-up with the fibres aligned in the load direction [37]. Additionally, the optimal value of t_H was defined numerically before the experiments, using the previously determined properties for the different fractures [37]. The patches were fabricated using four plies of CFRP prepreg (Texipreg HS 160 RM from SEAL®, Legnano, Italy) with 0.15 mm of ply thickness. Preparation of the bonding surfaces included abrasion and cleaning with compressed air (wood) or acetone (CFRP patch). The ductile adhesive Araldite 2015 was employed for all bonds. The repairs were fabricated in three

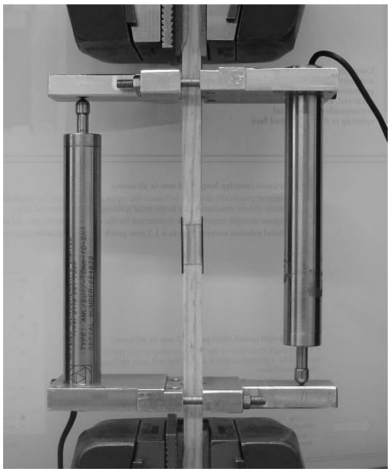

FIGURE 3 Experimental setup in the testing machine ($L_O = 5$ mm repair).

stages: bonding of the wood insert and bonding of the two patches separately. To assure the correct value of t_A, 0.2 mm diameter nylon fishing lines were used between the elements to be bonded. These lines were placed at the central overlap region, where it was observed numerically that the transmitted load is very low, in order to minimize the consequences of stress concentrations induced by the presence of the lines. The specimens were cured at room temperature. The tests were carried out in an Instron® 1125 (Norwood, MA, USA) testing machine with a 100 kN load cell, at room temperature and under displacement control (1 mm/min). Figure 3 shows the experimental setup for a $L_O = 5$ mm repair, using two linear variable differential transformers (LVDTs), providing the measurement of displacements for a length of approximately 170 mm. The average displacement between the two LVDTs was used to build the load-displacement (P-δ) curves. Six specimens were tested for each condition, guaranteeing at least four valid results.

4. NUMERICAL ANALYSIS

The FEM simulations were performed in ABAQUS®, considering two-dimensional models and geometrical non-linearities. Figure 4 represents the numerical idealization of the repair geometry described in Fig. 1 and loci of cohesive elements to simulate different fractures. Only one quarter of the repair was considered due to horizontal

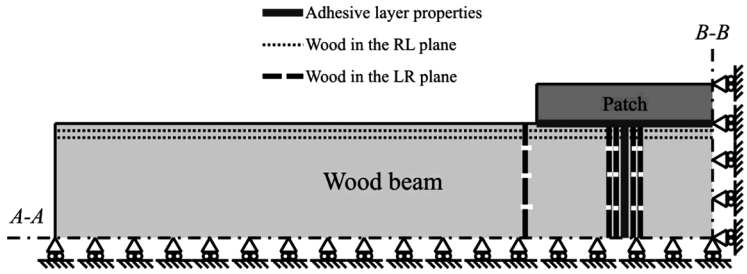

FIGURE 4 Numerical idealization and placement of the cohesive elements with different cohesive laws.

symmetry at the mid-thickness of the repair (line *A-A*) and vertical symmetry at their mid-length (line *B-B*). Figure 4 shows the placement of the elements representing the adhesive layer (between the patch and the wood components, and between the undamaged portions of the beam and the wood insert). Within the wood beam and insert, crack growth was considered in the *RL* and *LR* propagation planes. The fracture planes for both wood fractures were established based on experimental evidence from the test results and stress analysis on the potential critical regions. The possibility of horizontal *RL* propagations was included along the entire length of the repair near the patch bonding region (at 0.15 and 0.3 mm to the wood/adhesive interface). These boundary values were chosen as an approximation of the experimentally measured fracture loci on the tested specimens. Despite the fact that two planes were considered, if a numerical fracture within the wood should occur rather than in the adhesive layer, due to lower cohesive properties, it will most probably take place at the fracture plane nearest to the adhesive layer. This is due to the typical reduction of peel and shear stresses from the bond towards the inner regions of the repaired structure [38]. Vertical *LR* failures were considered within the wood structure and cohesive elements were inserted near the vertical bond, at similar distances to the bond interfaces, *i.e.*, 0.15 and 0.3 mm. However, in this region, the repair

TABLE 2 Elastic Properties of Wood and CFRP

Wood	E_L (GPa)	$E_R = E_T$ (GPa)	$\nu_{LR} = \nu_{LT}$	ν_{RT}	G_{LR} (GPa)	G_{LT} (GPa)	G_{RT} (GPa)
[36,39]	10.2	1.01	0.342	0.38	1.1	1.1	0.17
CFRP	E_1 (GPa)	$E_2 = E_3$ (GPa)	$\nu_{12} = \nu_{13}$	ν_{23}	G_{12} (GPa)	G_{13} (GPa)	G_{23} (GPa)
[40]	109	8.82	0.342	0.38	4.32	4.32	3.2

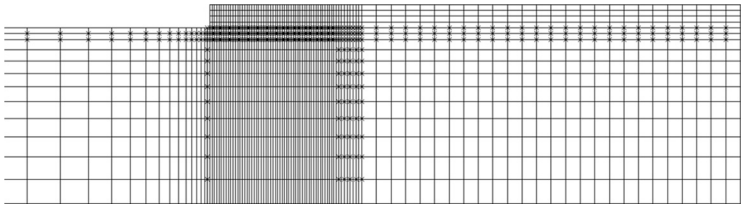

FIGURE 5 Mesh at the repaired region for the $L_O = 5$ mm repair.

will be expected to fail in the adhesive bond, which is significantly weaker in peel than this species of wood in the L-direction [23]. A possible cross-sectional failure of the wood member was also included near the patch edge. Other locations farther from the repair region were not included in the models since it was observed numerically that tensile stresses, responsible for a possible cross-sectional fracture of the wood member, peak slightly near the patch edge. Consequently, any cross-sectional failure would always occur near the repaired region. The mesh was built so that a modification of the failure path is possible between any crossing between failure paths (horizontal with vertical) to account for all possibilities. The wood and CFRP patches were modelled as elastic orthotropic materials, whose elastic properties are presented in Table 2. Figure 5 illustrates the mesh at the repaired region for the $L_O = 5$ mm repair (the fracture planes are represented by the small crosses). Plane-stress eight-node rectangular solid elements were used to model the wood and the patch. In the L-direction, the mesh was more refined along L_O, with 60 elements, since this is expected to be the region of highest stress gradients. A coarser mesh was considered for the wood insert. Outside the repaired region, bias effects were used towards the patch edge, due to slight stress concentrations expected at that region [41,42]. Twelve solid elements were used in the R-direction (thickness direction in Fig. 5), with an increasing refinement towards the horizontal fracture planes near the bond. The patch was modelled with four solid elements through thickness.

5. RESULTS

5.1. Numerical

The numerical failure modes for the repaired beams are described, aiming comparison with the experimental fractures. The behaviour of the $L_O = 5$, 10, and 15 mm repairs appeared to be equivalent. Figure 6 shows an example of this fracture for the (a) $L_O = 5$ mm

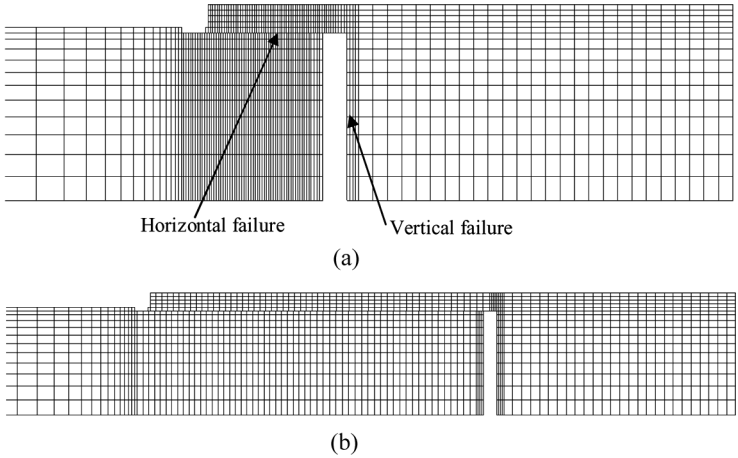

FIGURE 6 Numerical fractures for the (a) $L_O = 5$ mm and (b) $L_O = 15$ mm repairs.

and (b) $L_O = 10$ mm repairs. Notwithstanding the value of L_O, fracture was simultaneous horizontally along L_O in the wood beam at 0.15 mm of the wood/adhesive interface and vertically between the wood member and the insert as a cohesive failure of the adhesive layer. The horizontal fracture along L_O was triggered by a vertical crack (LR plane) near the patch edge, which then propagated horizontally. This failure could be anticipated from the knowledge of the typical stress behaviour of bonded assemblies, which experience a decreasing level of peel and shear stresses from the bond between repair constituents towards the inner regions of materials [38], explaining the horizontal fracture at 0.15 mm of the wood/adhesive interface instead of at 0.3 mm. The vertical failure at the bond between the wood member and the insert testifies to the lower strength of the adhesive in peel than the wood strength in the L-direction. This failure implies that the undamaged strength of the beams is not achieved for the values of L_O selected for the analysis, which would roughly correspond to a cross-sectional failure outside the repaired region. Thus, a numerical study was performed to evaluate the value of L_O that prompted a modification of the failure mechanism for a transverse cross-sectional failure near the patch edge. This modification implies that the repaired region becomes stronger than the parent material and that the repair approaches the undamaged strength of the wood member. Slightly smaller values are expected, though, because of the stress concentrations in the wood beam near the patch edge [41]. This fracture was attained for

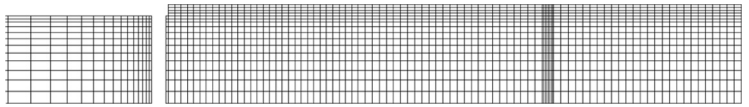

FIGURE 7 Numerical fracture for a repair with $L_O = 20.80$ mm.

$L_O = 20.80$ mm (Fig. 7), this being the value recommended on account of the maximization of the strength of the repair.

5.2. Experimental

The experimental fractures were revealed to be in good agreement with the simulations. Most of the undamaged wood beams fractured by a cross-sectional tensile failure (Fig. 8a). A few of the specimens failed near the grips due to stress concentrations at those regions, but these results were discarded. Similarly to the FEM results, failure was identical for the three values of L_O considered. In fact, all specimens fractured abruptly, without evidence of damage prior to failure. Figures 8b, c, and d show examples of fractured specimens for the $L_O = 5$, 10, and 15 mm repairs, respectively. In these repairs, fracture occurred concurrently as an *RL* propagation along L_O in the wood beam near the wood/adhesive interface and cohesively in the adhesive layer between the wood member and the insert. The horizontal *RL*

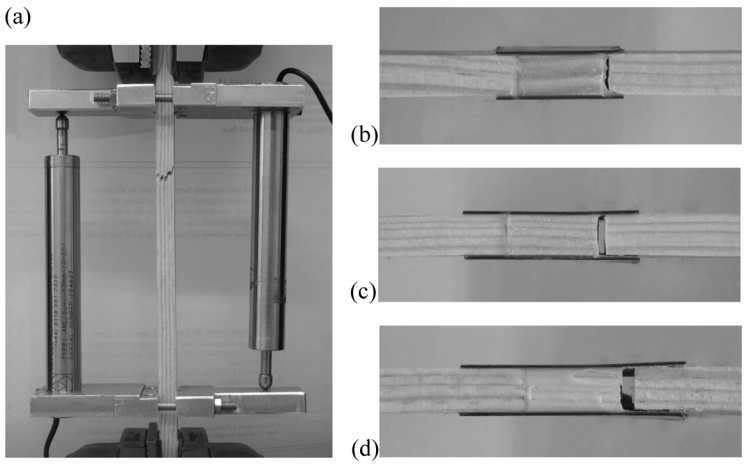

FIGURE 8 Example of experimental fractures for (a) the undamaged beam, and (b) $L_O = 5$ mm, (c) 10 mm, and (d) 15 mm repairs.

fracture was prompted by a vertical *LR* fracture near the patch edge, the same as the simulations.

5.3. Numerical/Experimental Comparison

A comparison between the numerical and experimental P-δ curves is initially shown in Fig. 9 ($L_O = 5$ mm repair) and Fig. 10 ($L_O = 10$ mm repair). The $L_O = 5$ mm repairs showed a practically linear behaviour up to failure, which was not the case for the $L_O = 10$ mm repairs where some non-linear behaviour is observed near the peak load. This is probably explained by non-linear behaviour of the wood occurring for $L_O = 10$ mm repairs, owing to the higher loads attained relative to $L_O = 5$ mm case. This aspect is not captured by the numerical simulations since wood was simulated as an elastic material. The initial stiffness also presents some scatter which can be considered normal in wood (natural material), since the elastic properties can vary drastically from specimen to specimen. Despite that, the numerical predictions were accurate in terms of maximum load. These figures also show a relatively small variation of this variable between specimens of the same repair configuration, which will be quantified. Figure 11 summarizes the results of maximum load (P_m), including the numerical predictions and the experimental average values and deviation. The numerical trend tends to replicate the overall tendency of P_m with L_O, assuming a linear variation between consecutive values of L_O. The

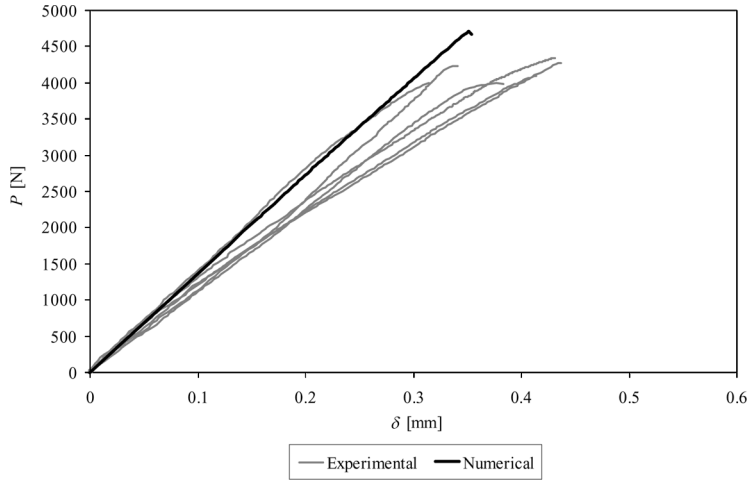

FIGURE 9 Experimental and numerical P-δ curves for the $L_O = 5$ mm repair.

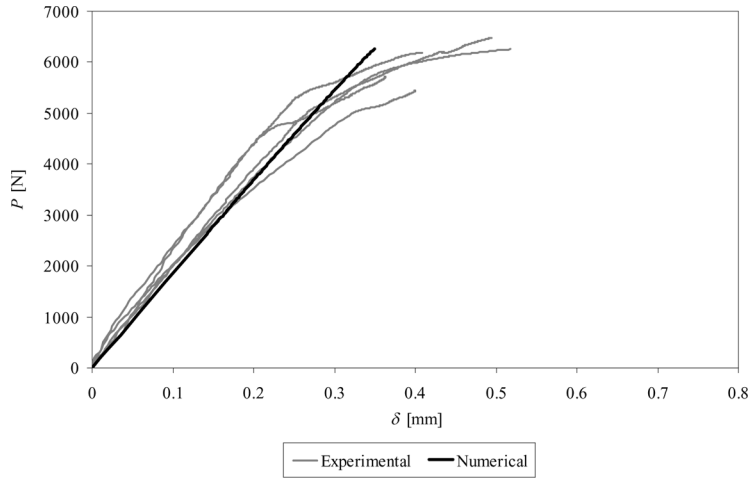

FIGURE 10 Experimental and numerical P-δ curves for the $L_O = 10\,\text{mm}$ repair.

predictions of P_m were found to be slightly above the average experimental values. However, apart from the $L_O = 5\,\text{mm}$ repair, these were always within the range of the experiments. The approximate difference of 11% between the numerical prediction and the average

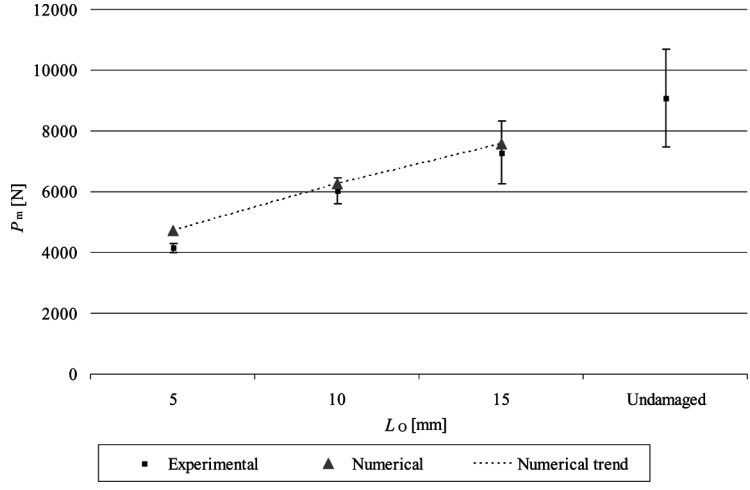

FIGURE 11 P_m as a function of L_P. Experimental results, numerical predictions, and respective tendency as a function of L_O.

experimental value for the $L_O = 5$ mm repair is not negligible and can be due to several issues, such as a higher influence of small deviations of the patch length on the strength of the repair or be caused by a bigger susceptibility to small misalignments or variations of t_A [43]. The experimental results for the undamaged beam showed a significantly larger deviation than for the repaired beams. This is understandable, since in the repaired beams P_m is also ruled by the adhesive properties, smearing the large variability of the wood properties on the global strength characteristics of the beams. Overall, the accurate numerical predictions prove the suitability of the FEM and CZMs for the strength prediction of the adhesively bonded repairs.

6. REPAIR OPTIMIZATION STUDY

Following the parametric study on L_O, an optimization technique consisting of adhesive filleting at the patch edges was tested in an attempt to increase the strength of the repairs. It is known that the stress singularities at square-edges may lead to adhesion failures and, consequently, to premature damage initiation [44,45]. The proposed solution aims at the reduction of through-thickness peel and shear peak stresses at those regions [46–51] and, as a result, to increase the strength of the repair. In terms of fabrication of the filleted repairs, some difficulties in the curing process can be expected, especially for low viscosity adhesives or if access is limited [52]. In this study, the fillets include all the patch thickness, minimizing through-thickness peel and shear peak stresses at the patch edges [53]. Bogdanovich and Kizhakkethara [54] performed a two-dimensional FEM study on double-strap joints with CFRP adherends under a tensile load, analysing the effect of straight and curved fillets on through-thickness peel and shear stresses in the adhesive layer. The numerical models used plane-strain elements and a sub-modelling technique was employed to extract stresses at the critical regions. The fillet was found to diminish significantly both peak stresses at the overlap edge near the fillet. Tsai and Morton [55] addressed the same issue experimentally and numerically using graphite-epoxy single-lap joints under tension. The Moiré interferometry method was used to extract shear strains near the fillet. It was concluded that a fillet effectively reduces shear strains and through-thickness peel and shear peak stresses near the fillet, subsequently increasing the joint strength. In this work, a straight 45° fillet angle was tested, being regarded as a near optimal configuration for bonded assemblies under tensile loads [40,56–58]. This geometric modification was tested for the three values of L_O evaluated (5, 10, and 15 mm). The numerical analysis followed the

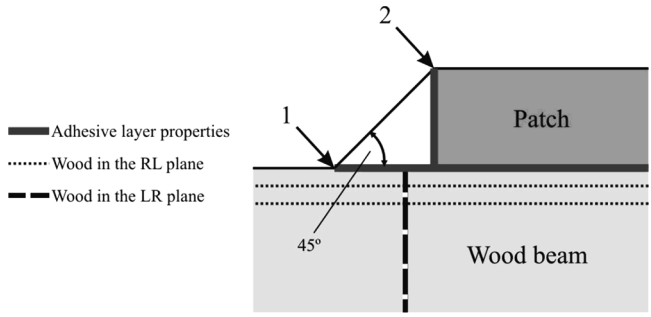

FIGURE 12 Loci of additional cohesive elements for the repairs with a fillet.

guidelines of Section 4. The adhesive fillet was modelled as a plastic isotropic material, with the respective properties obtained from a previous study [35]. Figure 12 illustrates the fillet geometry and loci of additional cohesive elements to simulate the fractures most likely to occur under tension [38,59]. Different locations were considered for these elements, with two possible damage initiation locations (1 and 2 in Fig. 12) and growth planes (vertically between the adhesive fillet and the patch and horizontally between the fillet and the wood beam). The failure mode was identical between all values of L_O. Figure 13 shows a mesh detail and fracture mode for the $L_O = 5$ mm repair. Fracture was identical to the repairs without a fillet (horizontally along L_O in the wood beam at 0.15 mm of the wood/adhesive interface and vertically in the adhesive layer between the wood member and the insert), concurrently with horizontal failure at path 1 between the fillet and the wood beam (Fig. 12). Compared with the repairs without a fillet, the $L_O = 5$, 10, and 15 mm repairs showed 3.9, 2.7, and 1.8% strength improvements, respectively. The relatively small improvements with the use of a fillet are due to the reduced value of t_H, which leads to a diminished shear area between the fillet and the wood beam [40]. Bigger values of t_H (relatively to L_O) can give improvements up to near

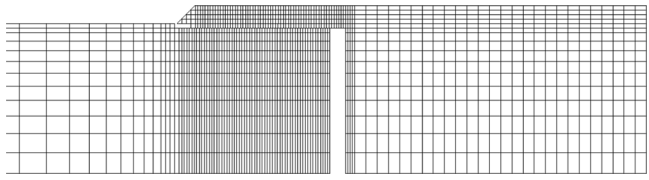

FIGURE 13 Numerical fracture for the $L_O = 5$ mm repair with a 45° straight fillet.

20% [60]. It should be emphasized that results for smaller fillet angles are not presented here, since, although they would provide a larger shear area, the numerical simulations showed a failure modification from initiation at path 1 to a premature failure at path 2 in Fig. 12 (vertically between the fillet and the patch) due to the increase of the fillet stiffness [38], preventing a strength improvement. Similar tendencies were found in the work of Belingardi *et al.* [57]. The reduction of the percentile strength improvement with L_O can be accounted for on the identical level of shear reinforcement provided by the adhesive fillet, since the fillet angle and value of t_H were kept constant. Future work will analyse the effect of filleting considering thicker patches and also will include the possibility of failure through the fillet which was demonstrated by Adams and Peppiatt [61] to be noticeably valuable.

7. CONCLUDING REMARKS

In this work, the tensile strength of adhesively bonded repairs with carbon-epoxy patches on wood members was addressed experimentally and numerically. The repair technique proposed consists of the replacement of the damaged wood portion with a wood insert and reinforcement with carbon-epoxy plates bonded at two opposite faces. A parametric analysis was carried out on the overlap length between the composite reinforcement and the undamaged portions of the beam. For the considered overlaps it was verified that failure loads increase linearly with overlap length. The numerical analysis used the finite element method and cohesive zone modelling to simulate damage initiation and propagation in different materials. To account for the experimental failures, damage propagation in the wood beam along two propagation planes was also simulated. The comparative analysis of the test results and the simulations showed a good correlation between both. Concerning the failure modes, even though several failure paths were introduced in the numerical models, these managed to reproduce the experimental failure mode accurately for all the conditions tested.

The validated numerical model was also used to verify the effect of filleting on these repairs. It was concluded that owing to the small patch thickness the strength improvement is negligible, does not increase with fillet angle reduction, and its percentile gain decreases with the increase of the overlap length.

ACKNOWLEDGMENTS

The authors would like to thank the Portuguese Foundation for Science and Technology for supporting the work presented here,

through the individual grant SFRH/BD/30305/2006 and the research project PDTC/EME-PME/64839/2006.

REFERENCES

[1] Schniewird, A. P. and Barret, J. D., *Wood Sci. Technol.* **6**, 43–47 (1972).
[2] Luong, M. P. *16th World Conference on Nondestructive Testing*, Montreal, Canada (2004).
[3] Bohannan, B., *Forest Prod. J.* **12**, 596–602 (1962).
[4] Sliker, A., *Forest Prod. J.* **12**, 91–96 (1962).
[5] Peterson, J., *J. Struct Eng.* **91**, 103–119 (1965).
[6] Lantos, G., *Wood Sci. Technol.* **2**, 136–143 (1970).
[7] Krueger, G. P., *Wood Sci. Technol.* **6**, 175–186 (1973).
[8] Stern, E. G. and Kumar, V. K., *Forest Prod. J.* **23**, 40–47 (1973).
[9] Hoyle, R. J., *Forest Prod. J.* **25**, 17–23 (1975).
[10] Kobetz, R. W. and Krueger, G. P., *Wood Sci. Technol.* **8**, 252–262 (1976).
[11] Bulleit, W. M., Sandberg, L. B., and Woods, G. J., *J. Struct Eng.* **115**, 433–444 (1989).
[12] Meier, U., Deuring, M., Meier, H., and Schwegler, G., *Proceedings of the First International Conference on Advanced Composite Materials on Bridges and Structures*, Sherbrooke, Québec, Canada, pp. 243–251 (1992).
[13] Triantafillou, T. C. and Deskovic, N., *J. Struct Eng.* **118**, 1270–1284 (1992).
[14] Plevris, N. and Triantafillou, T., *J. Struct Eng.* **121**, 174–186 (1995).
[15] Humphreys, M. F. and Francey, K. L., An investigation into the rehabilitation of timber structures with fibre composite materials. In: *Proceedings of Developments in Mechanics of Structures and Materials Conference*, Perth, Australia, December 2004, pp. 1317–1322.
[16] Triantafillou, T. C., *Prog. Struct. Eng. Mater.* **1**, 126–134 (1998).
[17] Radford, D. W., Van Goethem, D., Gutkowski, R. M., and Peterson, M. L., *Constr. Build. Mater.* **16**, 417–425 (2002).
[18] Wheeler, A. S. and Hutchinson, A. R., *Int. J. Adhes. Adhes.* **18**, 1–13 (1998).
[19] Neale, K. W., *Prog. Struct. Eng. Mater.* **2**, 133–138 (2000).
[20] Lopez-Anido, R., Michael, A. P., Sandford, T. C., and Goodell, B., *J. Perform. Constrtr. Fac.* **19**, 78–87 (2005).
[21] Raftery, G. M., Harte, A. M., and Rodd, P. D., *Int. J. Adhes. Adhes.* **29**, 580–588 (2009).
[22] Fiorelli, Juliano and Dias, Antonio Alves., Fiberglass-reinforced glulam beams: mechanical properties and theoretical model. *Mat. Res.* [online]. 2006, **9**, n.3, pp. 263–269. ISSN 1516–1439.
[23] Campilho, R. D. S. G., de Moura, M. F. S. F., Barreto, A. M. J. P., Morais, J. J. L., and Domingues, J. J. M. S., *Compos: Part A – Appl. S* **40**, 852–859 (2009).
[24] Campilho, R. D. S. G., de Moura, M. F. S. F., and Domingues, J. J. M. S., *Int. J. of Solids and Struct.* **45**, 1497–1512 (2008).
[25] Campilho, R. D. S. G., de Moura, M. F. S. F., Pinto, A. M. G., Morais, J. J. L., and Domingues, J. J. M. S., *Compos: Part B – Eng.* **40**, 149–157 (2009).
[26] Campilho, R. D. S. G., de Moura, M. F. S. F., Ramantani, D. A., Morais, J. J. L., and Domingues, J. J. M. S., *J. Adhes. Sci. Technol.* **23**, 1493–1513 (2009).
[27] Campilho, R. D. S. G., de Moura, M. F. S. F., Ramantani, D. A., Morais, J. J. L., and Domingues, J. J. M. S., *Int. J. Adhes. Adhes.* **29**, 678–686 (2009).
[28] Gustafson, P. A. and Waas, M., *Int. J. of Solids and Struct.* **46**, 2201–2215 (2009).

[29] Andersson, T. and Stigh, U., *Int. J. of Solids and Struct.* **41**, 413–434 (2004).
[30] Xie, D. and Waas, A. M., *Eng. Fract. Mech.* **73**, 1783–1796 (2006).
[31] Hogberg, J. L. and Stigh, U., *Eng. Fract. Mech.* **73**, 2541–2556 (2006).
[32] Leffler, K., Alfredsson, K. S., and Stigh, U., *Int. J. of Solids and Struct.* **44**, 530–545 (2007).
[33] de Moura, M. F. S. F., Campilho, R. D. S. G., and Gonçalves, J. P. M., *Compos. Sci. Technol.* **68**, 2224–2230 (2008).
[34] de Moura, M. F. S. F., Gonçalves, J. P. M., Chousal, J. A. G., and Campilho, R. D. S. G., *Int. J. Adhes. Adhes.* **28**, 419–426 (2008).
[35] Marques, E. A. S., da Silva, L. F. M., *J. Adhesion* **84**, 917–936 (2008).
[36] Silva, M. A. L., de Moura, M. F. S. F., and Morais, J. J. L., *Compos: Part A – Appl. S* **37**, 1334–1344 (2006).
[37] Bakis, C. E., Bank, L. C., Brown, V. L., Cosenza, E., Davalos, J. F., Lesko, J. J., Machida, A., Rizkalla, S. H., and Triantafillou, T. C., *J. Compos. Constr.* **6**, 73–87 (2002).
[38] Campilho, R. D. S. G, de Moura, M. F. S. F., Domingues, J. J. M. S., and Morais, J. J. L., *J. Adhes. Sci. Technol.* **22**, 1565–1591 (2008).
[39] Silva, M. A. L., Morais, J. J. L., de Moura, M. F. S. F., and Lousada, J. L., *Eng. Fract. Mech.* **74**, 2133–2147 (2007).
[40] Campilho, R. D. S. G., de Moura, M. F. S. F., and Domingues, J. J. M. S., *Compos. Sci. Technol.* **65**, 1948–1958 (2005).
[41] Deng, J. and Lee, M. M. K., *Compos.: Part B – Eng.* **39**, 731–739 (2008).
[42] Magalhães, A. G., de Moura, M. F. S. F., and Gonçalves, J. P. M., *Int. J. Adhes. Adhes.* **25**, 313–319 (2005).
[43] Kafkalidis, M. S. and Thouless, M. D., *Int. J. of Solids and Struct.* **39**, 4367–4383 (2002).
[44] Gleich, D. M., Van Tooren, M. J. L., and Beukers, A., *J. Adhes. Sci. Technol.* **15**, 1247–1259 (2001).
[45] Panigrahi, S. K. and Pradhan, B., *J. Adhes. Sci. Technol.* **21**, 379–398 (2007).
[46] Adams, R. D. and Harris, J. A., *Int. J. Adhes. Adhes.* **7**, 69–80 (1987).
[47] Hildebrand, M., *Int. J. Adhes. Adhes.* **14**, 261–267 (1994).
[48] da Silva, L. F. M. and Adams, R. D., *Int. J. Adhes. Adhes.* **27**, 227–235 (2007).
[49] da Silva, L. F. M. and Adams, R. D., *Int. J. Adhes. Adhes.* **27**, 216–226 (2007).
[50] Yan, Z. M., You, M., Yi, X. S., Zheng, X. L., and Li, Z., *Int. J. Adhes. Adhes.* **27**, 687–695 (2007).
[51] Chaves, F. J. P., da Silva, L. F. M., and de Castro, P. M. S. T., *Journal of Materials: Design and Applications* **222**, 159–174 (2008).
[52] Fitton, M. D. and Broughton, J. G., *Int. J. Adhes. Adhes.* **25**, 329–336 (2005).
[53] Lang, T. P. and Mallick, P. K., *Int. J. Adhes. Adhes.* **18**, 167–177 (1998).
[54] Bogdanovich, A. E. and Kizhakkethara, I., *Compos.: Part B – Eng.* **30**, 537–551 (1999).
[55] Tsai, M. Y. and Morton, J., *Compos. Struct.* **32**, 123–131 (1995).
[56] Rispler, A. R., Tong, L., Steven, G. P., and Wisnom, M. R., *Int. J. Adhes. Adhes.* **20**, 221–231 (2000).
[57] Belingardi, G., Goglio, L., and Tarditi, A., *Int. J. Adhes. Adhes.* **22**, 273–282 (2002).
[58] Campilho, R. D. S. G., de Moura, M. F. S. F., and Domingues, J. J. M. S., *Int. J. Adhes. Adhes.* **29**, 195–205 (2009).
[59] Apalak, M. K. and Engin, A., *J. Adhes. Sci. Technol.* **18**, 529–559 (2004).
[60] Quaresimin, M. and Ricotta, M., *Compos. Sci. Technol.* **66**, 176–187 (2006).
[61] Adams, R. D. and Peppiatt, N. A., *J. Strain Anal. Eng.* **9**, 185–196 (1974).